in redox potential existing between inhabited and non-inhabited sediment (Fig. 4*d*).

The *in-situ* studies from our sediment observatory revealed that the mud shrimp, *C. truncata*, although only 2-cm long, constructs unique burrows of extreme architectural and functional complexity that influence the whole sedimentology and geochemistry of the sea bed. The design of the upper burrow system, including mounds, funnels and first gallery, induces a hydrodynamic water exchange in the upper sediment layer. The biopumping of dissolved oxygen down to 60–80 cm sediment depth and the transport of detrital particles to similar depths can strongly accelerate the degradation of organic matter in the sandy sediments. □

Received 22 February; accepted 8 July 1996.

1. Berner, R. A. *Early Diagenesis: A Theoretical Approach* (Princeton Univ. Press, Princeton, 1980).
2. Revsbech, N. P., Jørgensen, B. B. & Blackburn, P. H. *Science* **207,** 1355–1356 (1980).
3. Aller, R. C. in *Animal–Sediment Relations* (eds McCall, P. L. & Tevesz, M. J. S.) 53–104 (Plenum, London, 1982).
4. Boudreau, B. P. *Geochim. Cosmochim. Acta* **58,** 1243–1249 (1994).
5. Aller, R. C. & Dodge, R. E. *J. Mar. Res.* **32,** 209–232 (1974).
6. Griffis, R. B. & Suchanek, T. H. *Mar. Ecol. Prog. Ser.* **79,** 171–183 (1991).
7. Dworschak, P. C. *Mar. Ecol.* **4,** 19–43 (1983).
8. Pemberton, S. G., Risk, M. J. & Buckley, D. E. *Science* **192,** 790–791 (1976).
9. Forster, S. & Graf, G. *Mar. Biol.* **123,** 335–346 (1995).
10. Ray, A. J. & Aller, R. C. *Mar. Geol.* **62,** 371–379 (1985).
11. Schlichting, H. *Boundary Layer Theory* 7th edn (McGraw-Hill, New York, 1987).
12. Huettel, M. & Gust, G. *Mar. Ecol. Prog. Ser.* **89,** 253–267 (1992).
13. Yager, P. L., Nowell, R. A. M. & Jumars, P. A. J. *J. Mar. Res.* **51,** 209–236 (1993).
14. Vogel, S. *Life In Moving Fluids* (Princeton Univ. Press, New Jersey, 1983).
15. Allanson, B. R., Skinner, D. & Imberger, J. *Est. Coast. Shelf Sci.* **35,** 253–266 (1992).
16. Revsbech, N. P. *Limnol. Oceangr.* **34,** 474–478 (1989).
17. Kristensen, E. J. *Coast. Res.* **1,** 109–116 (1985).
18. LaBarbera, M. & Vogel, S. *Limnol. Oceanogr.* **21,** 750–756 (1976).
19. Hall, P. O. J. & Aller, R. C. *Limnol. Oceanogr.* **37,** 1113–1119 (1992).
20. Hsü, K. J. *Physical Principles of Sedimentology* (Springer, Berlin, Heidelberg, 1989).

ACKNOWLEDGEMENTS. We thank T. Pillen and B. Unger for the construction and deployment of the diver observatory and for their help during underwater field work, other members of the Giglio Diving and Research Team: D. Claus, K. Eichstaedt, J. Hass and C. Lott; and A. Eggers, G. Eickert, O. Goerg, A. Glud, G. Herz, G. Kothe and V. Meyer for technical support and the construction of microelectrodes. The study was supported by the Max Planck Society.

CORRESPONDENCE and requests for materials should be addressed to W.Z. (e-mail: wiebke@postgate.mmi-mm.uni-bremen.de).

Genetically lean mice result from targeted disruption of the RIIβ subunit of protein kinase A

David E. Cummings, Eugene P. Brandon, Josep V. Planas, Kouros Motamed, Rejean L. Idzerda & G. Stanley McKnight

Department of Pharmacology, University of Washington School of Medicine, Seattle, Washington 98195–7750, USA

Cyclic AMP is an important second messenger in the coordinated regulation of cellular metabolism. Its effects are mediated by cAMP-dependent protein kinase (PKA), which is assembled from two regulatory (R) and two catalytic (C) subunits. In mice there are four R genes (encoding RIα, RIβ, RIIα, and RIIβ) and two C genes (encoding Cα and Cβ), expressed in tissue-specific patterns[1]. The RIIβ isoform is abundant in brown and white adipose tissue and brain, with limited expression elsewhere. To elucidate its functions, we generated RIIβ knockout mice. Here we report that mutants appear healthy but have markedly diminished white adipose tissue despite normal food intake. They are protected against developing diet-induced obesity and fatty livers. Mutant brown adipose tissue exhibits a compensatory increase in RIα, which almost entirely replaces lost RIIβ, generating an isoform switch. The holoenzyme from mutant adipose tissue binds cAMP more avidly and is more easily activated than wild-type enzyme. This causes induction of uncoupling protein and elevations of metabolic rate and body temperature, contributing to the lean phenotype. Our results demonstrate a role for the RIIβ holoenzyme in regulating energy balance and adiposity.

RIIβ null mutant mice were generated by targeted gene disruption; details of the knockout construction will be published elsewhere. Western blotting confirmed the absence of RIIβ protein in homozygous mutants. RIIβ mutants are fertile and long lived, exhibiting no overt abnormal phenotype. However, they have remarkably decreased white adipose tissue (WAT) mass. The weights of fat pads from three anatomical locations in mutants were about half those of the wild types (Table 1). Magnetic resonance imaging (Fig. 1*a*) confirmed that the reduction in fat occurs throughout the whole body. Whole-mouse magnetic resonance spectroscopy[2] and volume-of-distribution experiments with ^3H_2O showed that mutants have approximately 6% body fat, compared with 15% in the wild type.

The knockout mice are not cachectic. Overall weight is reduced by suggesting ~10%, that loss of fat is probably the only alteration in body composition (Table 1). Leanness does not seem to result from decreased food intake or absorption. Mutants tend to be slightly hyperphagic (Table 1), and show normal postprandial triglyceride blood levels. Plasma cholesterol, free fatty acids, insulin, glucose and thyroid hormones are also unperturbed (data not shown). The reduction of WAT seems to arise principally from decreased triglyceride stores, rather than diminished

TABLE 1 Knockout mice have reduced adipose tissue mass

	Reproductive fat-pad weight (% body weight)	Inguinal fat-pad weight (% body weight)	Retroperitoneal fat-pad weight (% body weight)	Reproductive fat-pad cellularity ($\times 10^{-6}$ cells per pad)	Inguinal fat-pad cellularity ($\times 10^{-6}$ cells per pad)	Retroperitoneal fat-pad cellularity ($\times 10^{-6}$ cells per pad)	Body weight (g)	Food intake (kcal per mouse per d)
Male								
Wild type	1.29 ± 0.10	0.96 ± 0.10	0.29 ± 0.04	17.4 ± 0.9	18.6 ± 1.9	3.7 ± 0.5	25.2 ± 0.9	11.4 ± 2.7
Mutant	0.62 ± 0.04	0.63 ± 0.04	0.11 ± 0.01	15.4 ± 1.5	21.4 ± 2.6	3.4 ± 0.5	23.4 ± 1.1	12.4 ± 1.5
% of wild type	48%	65%	37%	89%	115%	92%	93%	109%
	$P \leq 0.0001$	$P \leq 0.002$	$P \leq 0.0001$	$P = 0.14$	$P = 0.21$	$P = 0.31$	$P = 0.10$	$P = 0.39$
Female								
Wild type	2.25 ± 0.34	1.09 ± 0.03	0.23 ± 0.02	19.0 ± 2.0	21.6 ± 2.3	ND	22.4 ± 1.7	9.1 ± 0.4
Mutant	0.97 ± 0.13	0.72 ± 0.04	0.11 ± 0.02	17.4 ± 1.7	21.1 ± 2.8	ND	19.5 ± 0.8	10.9 ± 0.3
% of wild type	43%	66%	48%	92%	98%		87%	120%
	$P \leq 0.0006$	$P \leq 0.0001$	$P \leq 0.001$	$P = 0.21$	$P = 0.44$		$P = 0.06$	$P = 0.01$

RIIβ null mutants have reduced adipose tissue mass despite adequate food intake. Discrete white fat pads from three anatomical sites were dissected and weighed. 'Reproductive' refers to the epididymal and parametrial pads of males and females, respectively. White adipose tissue cellularity was ascertained by DNA quantitation. Consumption of standard mouse chow (Harlan Teklad) was measured over four months starting at six weeks of age. Results are means ± s.e.m.

adipocyte number, as revealed by the normal cellularity of fat pads (Table 1) and reduced adipocyte size (Fig. 1*b*). There are no obvious histological changes in tissues other than fat.

Mutants are protected against some of the adverse effects of consuming a high-fat diet. After eating a 58% fat diet for four months, normal mice became obese, whereas mutants remained lean (Fig. 1*d*). Furthermore, wild types developed fatty livers but mutants did not (Fig. 1*e*, *f*).

Mutants seem to be lean, at least in part because of changes in PKA activity and gene expression in brown adipose tissue (BAT). BAT facilitates non-shivering thermogenesis during cold acclimation[3] or chronic overeating[4]. This is accomplished by uncoupling protein (UCP), a proton translocator that uncouples mitochondrial respiration from oxidative phosphorylation in BAT, so that energy derived from oxidation of fatty acids is dissipated as heat, rather than stored as ATP. UCP is induced by a cAMP-dependent mechanism after β-adrenergic stimulation[5].

RIIβ is the principal PKA regulatory subunit in BAT. It is expressed more abundantly there than in any other tissue (data not shown). Although there are no histological changes in mutant BAT, loss of RIIβ protein is associated with a compensatory increase of the RIα isoform, normally scarce in this tissue (Fig. 2*a*). RIβ is not expressed in BAT, and RIIα is barely detectable in both wild type and mutants. Thus, elimination of RIIβ transforms the PKA in BAT from a predominantly RII-containing (type II) holoenzyme to a predominantly RI type. High-performance liquid chromatography (HPLC) separation of type I and II PKA confirms this isoform switch (Fig. 2*b*). The increased RIα compensates almost entirely for lost RIIβ, such that overall cAMP-binding capacity (a reflection of total R subunit quantity) is reduced by only ~10% (Fig. 3*a*). Total C subunit is decreased by roughly one third as measured by kinase activity (Fig. 3*b*) and western analysis (Fig. 2*a*). Thus it seems that an R:C ratio of at least 1:1 is maintained in mutant BAT. These changes in RIα and Cα arise by post-transcriptional mechanisms (P. S. Amieux and G.S.M., unpublished results).

In BAT, the largely type-I PKA in mutants binds cAMP more avidly than does the type-II PKA predominating in the wild type, with K_d values of 140 and 380 nM, respectively (Fig. 3*a*). Mutant PKA holoenzyme is consequently more readily activated by cAMP than is wild-type enzyme (K_a values of 80 and 350 nM, respectively, Fig. 3*b*). Accordingly, basal PKA activity is elevated by roughly five times in mutant BAT (Fig. 3*b*, insert). cAMP levels in wild-type and mutant BAT showed no differences that might be

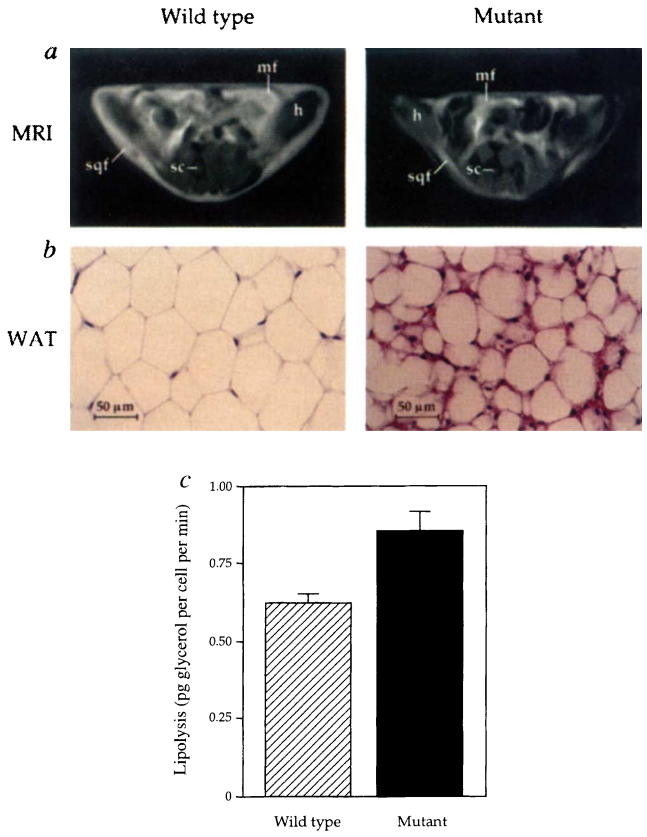

FIG. 1 RIIβ mutants have reduced fat throughout their bodies and resist diet-induced obesity. *a*, Fat-selective magnetic resonance images of female mice. Spin echo inversion-recovery sequences weighted by the magnetic relaxation time constant T1 are shown, in which only adipose tissue appears white. Images are 3-mm thick axial sections at the base of the hind legs. Similar results were obtained throughout the body. Abbreviations: mf, mesenteric fat; sqf, subcutaneous fat; sc, spinal cord; h, proximal hind leg. *b*, Representative histology of normal WAT, composed of large, polygonal cells with prominent triglyceride depots (clear spaces) and flattened nuclei. Comparable RIIβ mutant WAT reveals smaller, rounded adipocytes with diminished triglyceride stores, more eosinophilic aqueous cytoplasm, plumper nuclei, and scattered multivesicular cells. Sections were formalin fixed, paraffin embedded, and stained with haematoxylin and eosin. *c*, RIIβ mutant WAT has increased lipolysis, as assessed by glycerol release. Washed epididymal fat-pad fragments were gently shaken at 37 °C in Krebs Ringer–HEPES buffer (pH 7.2) with 1% bovine serum albumin. Glycerol content of the medium was determined at six time points over two hours using an enzymatic assay (Sigma); cell number was assessed by DNA quantification. Results are means ± s.e.m. from five pairs of mice ($P = 0.01$). *d*, RIIβ mutants resist diet-induced obesity. Combined weights of bilateral epididymal, inguinal and retroperitoneal fat pads form 6 mice per group were measured after four months on either an 11% or 58% lipid diet[25]. On the high-fat diet normal mice developed markedly increased adiposity, whereas mutants remained lean. Overall body weights of both groups were only slightly increased. *e*, *f*, Mutants are protected from developing fatty livers on the high-fat diet. Hepatic triglycerides were quantified in five wild-type and five mutant mice with an enzymatic assay (Boehringer Mannheim). Values are means ± s.e.m. ($P = 0.001$). Haematoxylin and eosin-stained liver sections were counterstained with oil-red-O to reveal abnormal lipid deposits (bright red) in hepatocytes of normal animals. This pathology is absent in mutants. Specialized mouse food was provided by Research Diets, Inc. By calories, the low-fat diet contained 60% corn starch and 7% hydrogenated coconut oil, whereas the high-fat diet contained 13% corn starch and 54% coconut oil. Both diets contained 12% maltodextrin, 4% soybean oil, 16% casein, and identical vitamins and minerals.

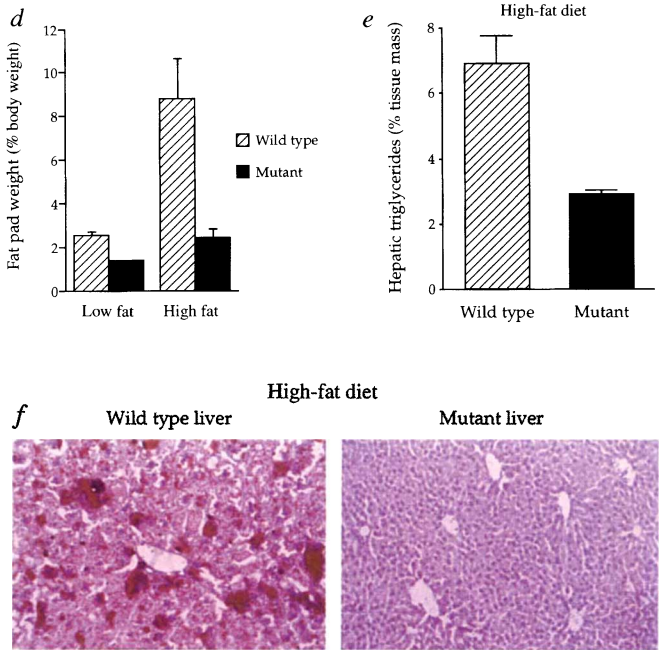

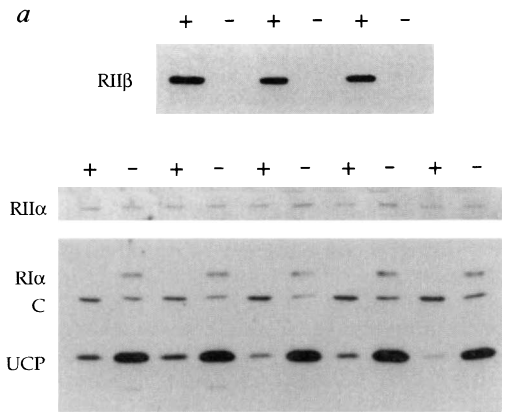

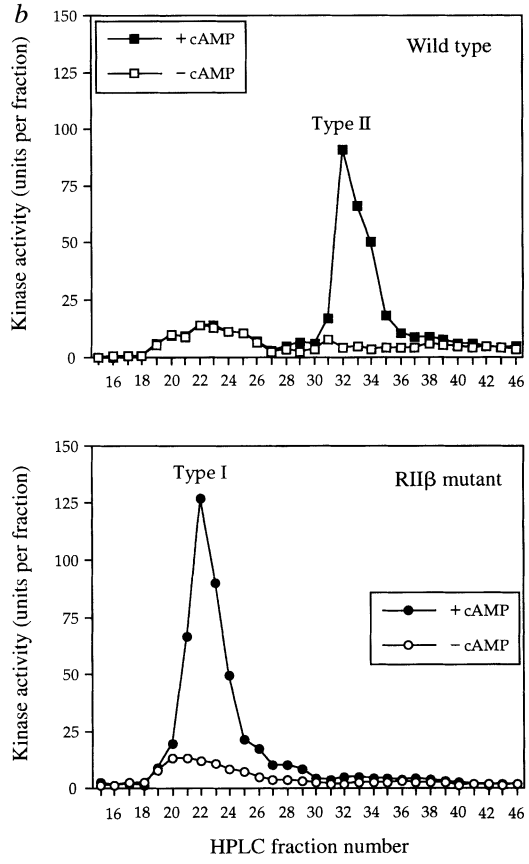

FIG. 2 *a*, Changes in protein levels and PKA activity in RIIβ mutant BAT. Western blots of BAT from wild-type (+) and knockout (−) mice were probed with the antibodies shown. Elimination of RIIβ in mutants is confirmed by the complete absence of RIIβ protein in BAT. The RIα isoform is markedly increased in mutants, whereas there is a small loss of C subunit. RIβ is not detectable in either wild-type or mutant adipose tissue. RIIα is barely detectable, and is unaltered in mutants. UCP is increased 4–5-fold in mutants, as revealed by scanning densitometry. *b*, Mutant BAT displays an isoform switch from type II to type I PKA. Type I (fractions 20–25) and type II (fractions 31–35) PKA from BAT homogenates were resolved by ion exchange chromatography. Displayed are basal (−cAMP) and total activatable (+cAMP) kinase activity.

METHODS. BAT protein homogenates (40 μg per lane) were resolved by 10% SDS–PAGE and transferred to nitrocellulose. Coomassie Blue staining confirmed uniformity of the protein loading. Immunoblotting was performed with polyclonal antisera raised against recombinant murine PKA subunits and diluted as follows: RIIβ 1:10,000; RIIα 1:1,000; RI 1:200; and C 1:2,000. The anti-RI antisera recognizes both RIα and RIβ, which are resolvable using this gel system; the anti-C antibody recognizes both Cα and Cβ, which co-migrate. Anti-RIIβ and RIIα antisera were provided by J. Scott, and anti-hamster UCP (1:2,000) by L. Kozak. Primary antibodies were visualized with horseradish peroxidase-coupled goat anti-rabbit Ig (1:40,000) and ECL (Amersham). Ion exchange chromatography was performed as previously described[26]. BAT protein (4 mg) was loaded onto DEAE columns and separated by HPLC with a linear salt gradient from 0 to 250 mM NaCl. Kinase activity of individual fractions was determined with Kemptide substrate as previously described[27], in the presence or absence of 5 μM cAMP. Type I PKA elutes between 40 and 80 mM NaCl (fractions 20–25), and type II between 130 and 180 mM NaCl (fractions 31–35). Free C subunit elutes just before type I holoenzyme.

attributed to extrinsic (for example, sympathetic) stimulation (data not shown). These data suggest that the changes in PKA activity result from the type II to type I isoform switch, rather than from a gross deregulation of C subunits due to either loss of R subunits or increased cAMP.

The elevated basal PKA activity leads to a four- to fivefold increase in UCP (Fig. 2*a*), at least partly by inducing UCP messenger RNA (data not shown). Figure 3*c*, *d* shows that knockouts have an elevated metabolic rate (assessed by oxygen consumption, which closely reflects energy expenditure[6]), and a 0.8 °C increase in body temperature (Fig. 3*e*). These findings suggest that excess UCP in BAT, arising from increased basal PKA tone, renders RIIβ-mutant mice metabolically inefficient, causing food calories to be wasted as heat and depleting fat stores. Furthermore, lipoprotein lipase mRNA in BAT (whose expression is also PKA dependent[7]) seems to be overexpressed, possibly helping mutant BAT to compete with WAT for dietary triglycerides, to be burned rather than stored.

After BAT, RIIβ is most highly expressed in WAT, where it is also the principal PKA regulatory isoform (data not shown). In this tissue, PKA transduces signals from catecholamines and glucagon to stimulate lipolysis and inhibit lipogenesis. Like BAT, RIIβ mutant WAT displays increased RIα, a type II to I isoform switch, and elevated basal PKA activity despite moderately decreased total PKA activity and C-subunit protein (data not shown). These changes are associated with a 35% increase in basal lipolysis in cultured adipocytes (Fig. 1*c*), which may contribute to the lean phenotype. However, serum glycerol and free fatty acids were similar in wild-type and mutant mice. As both BAT and WAT are affected in RIIβ mutants, we are unable to determine their relative contributions to the lean phenotype without generating a tissue-specific RIIβ defect.

Important advances in understanding body-weight regulation have resulted from the study of genetically obese rodent strains[8–12], of which there are at least 12 (refs 13–15). RIIβ mutants are one of only a few animal models of genetic leanness[16–18]. Several obese rodent strains have reduced UCP and thermogenically inactive BAT, in contrast to RIIβ mutants[3]. It will be interesting to see if the RIIβ knockout can rescue an obese phenotype when two mutant strains are interbred.

RIIβ mutants have markedly reduced leptin mRNA and plasma levels (data not shown), corroborating the proposed role of leptin as an adiposity indicator[8]. Leptin is also thought to be a satiety factor[19–21]. However, only mild hyperphagia, insufficient to maintain normal adiposity, is seen in RIIβ mutants despite reduced leptin levels. A change in the mutants' body-weight regulatory system could exist, preventing them from developing fully compensatory hyperphagia. It has been proposed that BAT might produce an appetite-suppressing signal[22], because of the unexpected finding that BAT-deficient mice develop hyperphagia[14]. It is possible that such a factor is induced in the overactive BAT of RIIβ mutants, inhibiting them from eating enough to maintain normal lipid stores.

One way that the brain is thought to regulate adiposity is by modulating sympathetic stimulation of PKA in BAT to control facultative energy expenditure through UCP[3]. RIIβ mutants provide evidence for this phenomenon, as their elevated basal PKA activity in BAT is associated with increased UCP, excess

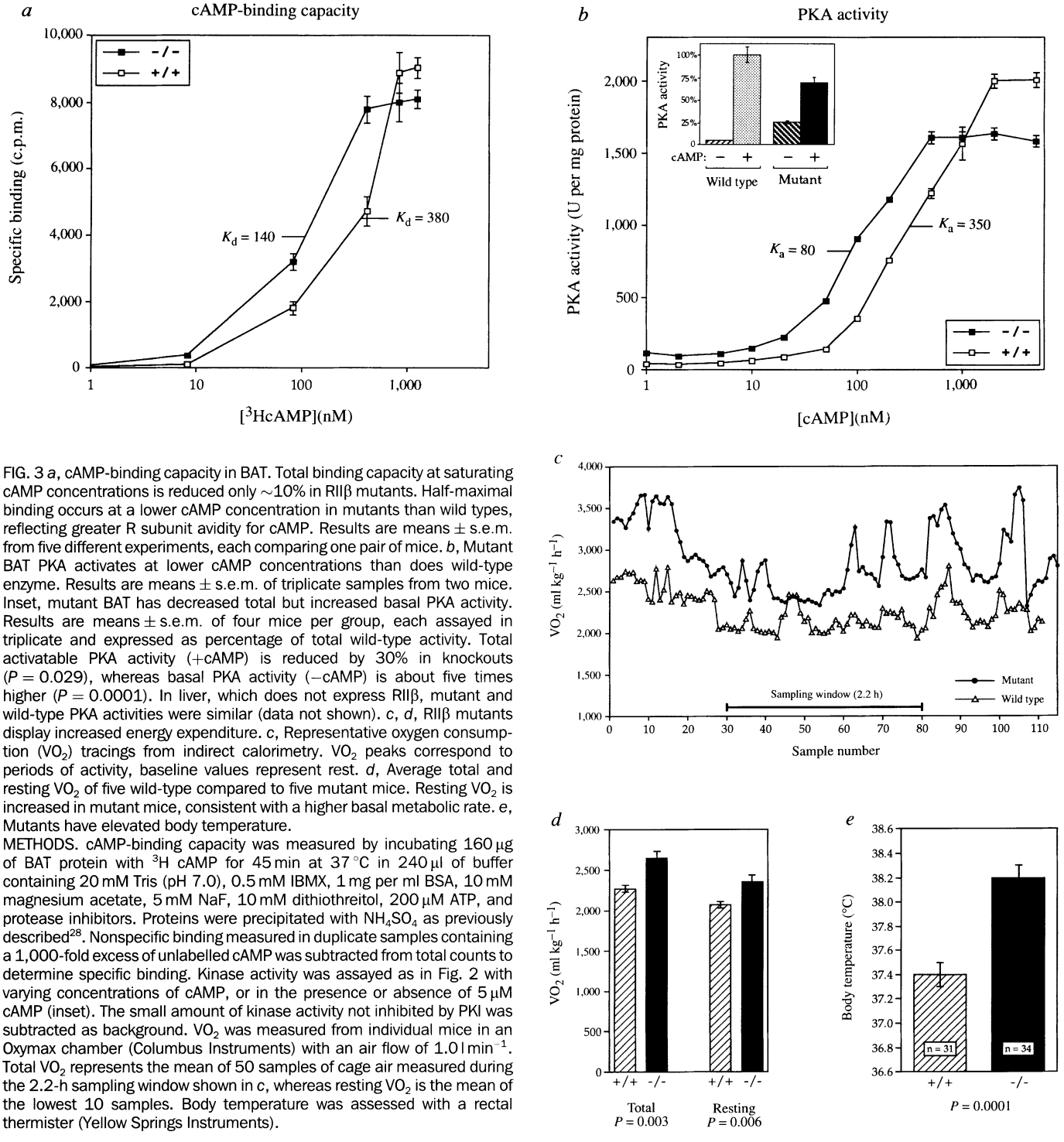

FIG. 3 *a*, cAMP-binding capacity in BAT. Total binding capacity at saturating cAMP concentrations is reduced only ~10% in RIIβ mutants. Half-maximal binding occurs at a lower cAMP concentration in mutants than wild types, reflecting greater R subunit avidity for cAMP. Results are means ± s.e.m. from five different experiments, each comparing one pair of mice. *b*, Mutant BAT PKA activates at lower cAMP concentrations than does wild-type enzyme. Results are means ± s.e.m. of triplicate samples from two mice. Inset, mutant BAT has decreased total but increased basal PKA activity. Results are means ± s.e.m. of four mice per group, each assayed in triplicate and expressed as percentage of total wild-type activity. Total activatable PKA activity (+cAMP) is reduced by 30% in knockouts ($P = 0.029$), whereas basal PKA activity (−cAMP) is about five times higher ($P = 0.0001$). In liver, which does not express RIIβ, mutant and wild-type PKA activities were similar (data not shown). *c*, *d*, RIIβ mutants display increased energy expenditure. *c*, Representative oxygen consumption (VO_2) tracings from indirect calorimetry. VO_2 peaks correspond to periods of activity, baseline values represent rest. *d*, Average total and resting VO_2 of five wild-type compared to five mutant mice. Resting VO_2 is increased in mutant mice, consistent with a higher basal metabolic rate. *e*, Mutants have elevated body temperature.

METHODS. cAMP-binding capacity was measured by incubating 160 μg of BAT protein with ^{3}H cAMP for 45 min at 37 °C in 240 μl of buffer containing 20 mM Tris (pH 7.0), 0.5 mM IBMX, 1 mg per ml BSA, 10 mM magnesium acetate, 5 mM NaF, 10 mM dithiothreitol, 200 μM ATP, and protease inhibitors. Proteins were precipitated with NH_4SO_4 as previously described[28]. Nonspecific binding measured in duplicate samples containing a 1,000-fold excess of unlabelled cAMP was subtracted from total counts to determine specific binding. Kinase activity was assayed as in Fig. 2 with varying concentrations of cAMP, or in the presence or absence of 5 μM cAMP (inset). The small amount of kinase activity not inhibited by PKI was subtracted as background. VO_2 was measured from individual mice in an Oxymax chamber (Columbus Instruments) with an air flow of 1.0 l min^{-1}. Total VO_2 represents the mean of 50 samples of cage air measured during the 2.2-h sampling window shown in *c*, whereas resting VO_2 is the mean of the lowest 10 samples. Body temperature was assessed with a rectal thermister (Yellow Springs Instruments).

energy expenditure, and leanness. In contrast, mice made deficient in BAT with a toxigenic transgene develop an abnormally efficient metabolism and obesity[14]. Chronic sympathetic stimulation normally causes BAT hypertrophy[23]. However, wild-type and mutant interscapular BAT showed no differences in weight (65 ± 17 compared to 60 ± 17 mg, respectively) or DNA content (119 ± 7 compared to 123 ± 5 μg), and mutant tissue had only slightly increased protein content (8.8 ± .5 compared to 10.9 ± 1.2 mg). In mice, adrenergic stimulation of β1 receptors is felt to be the principal mediator of BAT hypertrophy, whereas β3 receptors are probably most important for UCP induction[23]. PKA changes in RIIβ mutant BAT mimic β3 more than β1 stimulation, because they do not cause hypertrophy.

Chronic activation of PKA in adipose tissue through β-adrenergic stimulation is being investigated as a mode of obesity therapy. Research has focused on agonists specific for β_3 receptors[24], which are adipose specific[23]. Our results raise the possibility that RIIβ could also provide a target for anti-obesity drugs. □

Received 30 May; accepted 24 June 1996.

1. McKnight, G. S. *Curr. Opin. Cell Biol.* **3,** 213–217 (1991).
2. Stein, D. T., Babcock, E. E., Malloy, C. R. & McGarry, J. D. *Int. J. Obes. relat. metab. Disord.* **19,** 804–810 (1995).
3. Himms-Hagen, J. *FASEB J.* **4,** 2890–2898 (1990).
4. Rothwell, N. J. & Stock, M. J. *Nature* **281,** 31–35 (1979).
5. Kopeck'y, J. *et al. J. biol. Chem.* **265,** 22204–22209 (1990).
6. Jequier, E. & Felber, J.-P. *Baillière's clin. Endocr. Metab.* **1,** 911–935 (1987).
7. Carneheim, C., Nedergaard, J. & Cannon, B. *Am. J. Physiol.* **254,** E155–E161 (1988).

8. Zhang, Y. *et al. Nature* **372,** 425–432 (1994).
9. Chen, H. *et al. Cell* **84,** 491–495 (1996).
10. Lee, G.-H. *et al. Nature* **379,** 632–635 (1996).
11. Chua, S. C. *et al. Science* **271,** 994–997 (1996).
12. Noben-Trauth, K., Naggert, J. K., North, M. A. & Nishina, P. M. *Nature* **380,** 534–538 (1996).
13. Friedman, J. M. & Leibel, R. L. *Cell* **96,** 217–220 (1992).
14. Lowell, B. B. *et al. Nature* **366,** 740–742 (1993).
15. Tecott, L. H. *et al. Nature* **374,** 542–546 (1995).
16. Schneider, A., Davidson, J.J., Wullrich, A. & Kilimann, M. W. *Nature Genet.* **5,** 381–385 (1993).
17. Katz, E. B., Stenblt, A. E., Hatton, K., DePinho, R. & Charron, M. J. *Nature* **377,** 151–155 (1995).
18. Kozak, L. P., Kozak, U. C. & Clarke, G. T. *Genes Dev.* **5,** 2256–2264 (1991).
19. Pelleymounter, M. A. *et al. Science* **269,** 540–543 (1995).
20. Halaas, J. L. *et al. Science* **269,** 543–546 (1995).
21. Campfield, L. A., Smith, F. J., Guisez, Y., Devos, R. & Burn, P. *Science* **269,** 546–549 (1995).
22. Flier, J. S. *Cell* **80,** 15–18 (1995).
23. Lafontan, M. & Berlan, M. *J. Lipid Res.* **34,** 1057–1091 (1993).
24. Arner, P. *New Engl. J. Med.* **333,** 382–383 (1995).
25. Surwit, R. S. *et al. Metabolism* **44,** 645–651 (1995).
26. Clegg, C. H., Cadd, G. G. & McKnight, G. S. *Proc natn. Acad. Sci. U.S.A.* **85,** 3703–3707 (1988).
27. Clegg, C. H., Correll, L. A., Cadd, G. G. & McKnight, G. S. *J. biol. Chem.* **262,** 13111–13119 (1987).
28. Doskeland, S. O. & Ogreid, D. *Meth. Enzym.* **159,** 147–150 (1988).

ACKNOWLEDGEMENTS. We thank K. Millet, T. Su and K. Gerhold for technical assistance; S. Woods and C. Park for calorimetry guidance; E. Shankland for assistance with MRI; and R. Palmiter, M. Schwarz and D. Porte for comments on the manuscript.

CORRESPONDENCE and requests for materials should be addressed to G.S.M. (e-mail: mcknight@u.washington.edu).

Where in the brain does visual attention select the forest and the trees?

G. R. Fink*, P. W. Halligan†‡, J. C. Marshall‡, C. D. Frith*, R. S. J. Frackowiak* & R. J. Dolan*§

* Wellcome Department of Cognitive Neurology, Institute of Neurology, 12 Queen Square, London WC1N 3BG, UK
† Rivermead Rehabilitation Centre, Abingdon Road, Oxford OX1 4XD, UK
‡ Neuropsychology Unit, University Department of Clinical Neurology, The Radcliffe Infirmary, Woodstock Road, Oxford OX2 6HE, UK
§ Royal Free Hospital School of Medicine, Roland Hill Street, London NW3 2PF, UK

THE perceptual world is organized hierarchically: the forest consists of trees, which in turn have leaves. Visual attention can emphasize the overall picture (global form) or the focal details of a scene (local components)[1]. Neuropsychological studies have indicated that the left hemisphere is biased towards local and the right towards global processing. The underlying attentional and perceptual mechanisms are maximally impaired by unilateral lesions to the temporal and parietal cortex[2,3]. We measured brain activity of normal subjects during two experiments using 'hierarchically' organized figures. In a directed attention task, early visual processing (prestriate) areas were activated: attention to the global aspect of the figures activated the right lingual gyrus whereas locally directed attention activated the left inferior occipital cortex. In a subsequent divided attention task, the number of target switches from local to global (and vice versa) covaried with temporal–parietal activation. The findings provide direct evidence for hemispheric specialization in global and local perception; furthermore, they indicate that temporal–parietal areas exert attentional control over the neural transformations occurring in prestriate cortex.

We measured brain activity, indexed by regional cerebral blood flow (rCBF), in two separate experiments using 'hierarchically' organized visual stimuli (Fig. 1). In the first experiment, subjects were asked to attend to and name either the global or the local aspect of the figures in separate blocks of trials. As psychophysical differences in global and local processing may be confounded by differences in stimulus size[4], we controlled for size effects by presenting both large and small hierarchical figures in a factorial experimental design. In the second experiment, a preselected target letter appeared at either the global or the local level and the subjects were required to say at which of the two levels the target had appeared. The number of times that the target switched from the global to the local level (or vice versa) on successive trials varied parametrically across the experiment.

In the first experiment, as predicted, marked differences in neuronal activation associated with figure size were observed in the striate (primary visual) cortex: large stimuli were associated with extensive striate activation and small stimuli with more restricted posterior (foveal) striate activations ($P < 0.05$, using statistical parametric mapping and corrected for multiple non-independent comparisons). In addition, when subjects attended to the global aspect of figures, significant increases in relative rCBF were seen in the right lingual gyrus (Brodmann area 18; $P < 0.05$, corrected; Table 1, Fig. 2). When subjects attended to the local attribute, there was a significant relative rCBF increase in the left inferior occipital cortex (BA 18; $P < 0.05$, corrected, Table 1, Fig. 2). A direct comparison of rCBF changes between the two hemispheres indicated that these lateralized effects were statistically significant ($P < 0.01$). A significant interaction between figure size and the activation due to local processing was observed in the left inferior occipital cortex (BA 18, Fig. 2) alone, where the difference

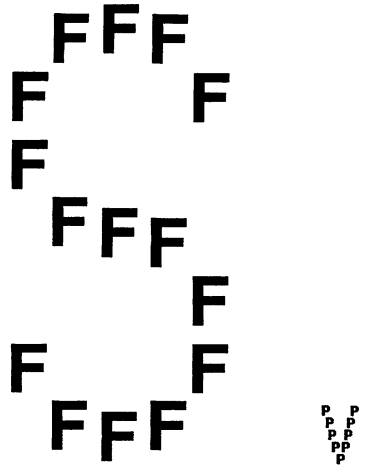

FIG. 1 Example of figures used as stimuli during the global and local processing experiments. The S and the V represent the global level and the F and the P the local level. All figures used were non-congruent for the global and local level. During the rCBF measurements, the figures were shown every 1.5 s for 300 ms in the centre of a 14 inch video display unit at a viewing distance of 40 cm. In the first experiment, 12 different letters were used to create the figures. These were presented in a quasi-random sequence that prevented the same letter appearing at the local or global level on successive trials[16]. To study stimulus size effects on global and local processing, both large figures (170 × 72 mm, made of letters 21 × 13 mm, visual angle subtended 24° and 10°) and small figures (30 × 14 mm, made of letters 3.5 × 2.5 mm, visual angle 4° and 2°) were used. Subjects were instructed to attend to either the global or the local level and to name the appropriate letter. rCBF measurements were performed during the following four conditions: global directed attention, large stimuli; local directed attention, large stimuli; global directed attention, small stimuli; local directed attention, small stimuli. Subjects lay with eyes open in a quiet, darkened room. Twelve rCBF measurements were performed per subject (three repeats per condition); globally and locally directed attention tasks were alternated. During the second experiment (divided attention), the same stimuli, (large letters only), presentation rate and number of measurements were used, however, this time a preselected target letter appeared at either the global or the local level. The number of switches between perceptual levels was varied on successive trials from 1 to 34 per min. The number of times that a given target letter occurred at the global or the local level was kept roughly equal across the rCBF measurements. A quasi-random sequence prevented the same stimulus from occurring on successive trials.